Electrophoretic co-deposition of Mn1.5Co1.5O4, Fe2O3 and CuO: Unravelling the effect of simultaneous addition of Cu and Fe on the microstructural, thermo-mechanical and

(Article begins on next page)

21 August 2024

Electrophoretic co-deposition of Mn$_{1.5}$Co$_{1.5}$O$_4$, Fe$_2$O$_3$ and CuO: unravelling the effect of simultaneous addition of Cu and Fe on the microstructural, thermo-mechanical and corrosion properties of in-situ modified spinel coatings for solid oxide cell interconnects

E. Zanchi [1], J. Ignaczak [2], S. Molin [2], G. Cempura [3], A. R. Boccaccini [4], F. Smeacetto [1*]

[1] Department of Applied Science and Technology, Politecnico di Torino, Corso Duca degli Abruzzi 24, Torino 10129, Italy

[2] Faculty of Electronics, Telecommunications and Informatics, Gdansk University of Technology, ul. G. Narutowicza 11/12, Gdansk 80-233, Poland

[3] AGH University of Science and Technology, al. Mickiewicza 30, Krakow 30-059, Poland

[4] Department of Materials Science and Engineering, University of Erlangen-Nuremberg, Cauerstr. 6, Erlangen 91058, Germany

*Corresponding author: federico.smeacetto@polito.it

Abstract

A systematic microstructural, thermo-mechanical and electrical characterization of simultaneous Fe–Cu doped Mn–Co spinel coatings processed by electrophoretic co-deposition on Crofer 22 APU is here reported and discussed. An innovative approach for the simultaneous electrophoretic deposition of three spinel precursors is designed, conceived and optimised, with the aim of outlining time- and energy-saving spinel modification routes. The effect of different levels of Cu and Fe co-doping is observed on the stability of the modified Mn–Co spinel phase, the coefficient of thermal expansion (CTE), the corrosion resistance and on the densification behaviour of the obtained coatings. Cu determines an increase of CTE, while Fe has the opposite behavior. The synergic effect of the simultaneous Fe and Cu co-doping results in an improved densification and the stabilization of the MnCo$_2$O$_4$ cubic phase. The most interesting results in terms of corrosion resistance are obtained for the Mn$_{1.28}$Co$_{1.28}$Fe$_{0.15}$Cu$_{0.29}$O$_4$ spinel.

1

Introduction

New low carbon technologies for clean hydrogen production and conversion require fundamental advances in design and processing of advanced and functional ceramics. Solid oxide cells (SOCs) devices are of great interest due to their high efficiency either as clean power generators (SOFC) and convertors of surplus renewable electricity to green hydrogen (SOEC) that can further be converted to synthetic clean fuels and chemicals [1]. The core of this technology is the stack, where the ceramic cells and the stainless steel interconnects are stacked together to reach the desired performance. The degradation of stainless steel interconnects is one of the main issues limiting the durability and highly compromising the efficiency and the performance of SOC stacks [2–4]. Ceramic protective coatings are widely used in order to reduce the chromium evaporation and the excessive growth of the oxide scale on the interconnect, which determines an increase of the electrical resistance [5]. The overall performance of a ceramic protective coating is related to its high electronic conductivity, the coefficient of thermal expansion and Cr and O_2-blocking capability. Materials in the Mn–Co spinel family are considered the state of the art coating materials [6,7]. Furthermore, the properties of the Mn–Co-based spinels can be tuned and improved by substituting part of the spinel elements by transition metals such as Fe and Cu [8–12]. Spinel protective coatings have been deposited by different methods, such as sputtering, screen printing, thermal and plasma spray, slurry deposition, dip coating and electrophoretic deposition (EPD) [5,13–15]. EPD offers the possibility to deposit homogeneous layers in a short time at RT condition with a simple and adaptable setup, thus making EPD a cost-effective technique suitable for industrial applications [16,17]. Anyway, the quality of the obtained coatings strongly depends on the engineering of the EPD suspensions, the optimization of the deposition parameters and the choice of an appropriate sintering route [18–20].

2

In our previous works we demonstrated the possibility to process Cu-doped Mn–Co spinels by EPD co-deposition [21,22]. The addition of Cu improves the coating density; the long-term stability of the Mn-Co-Cu spinel coatings with respect to their effectiveness in providing corrosion protection and Cr diffusion limitation were demonstrated.

In parallel, we reported a microstructural and electrical characterization of Fe-doped Mn–Co spinel coatings processed by electrophoretic co-deposition of Mn-Co spinel and Fe_2O_3 powders on Crofer 22 APU and AISI 441 steel substrates [12,23]. Specifically, we discussed the different mechanisms by which iron doping of Mn–Co spinels can influence elemental interdiffusion at the steel-oxide scale-coating interfaces and relative contributions to the overall area specific resistance. The Fe doped Mn–Co coatings lead to the formation of a thinner oxide scale, significantly improving the oxidation resistance.

However, a comprehensive assessment of the simultaneous Cu and Fe addition into the Mn-Co spinel dual phase structure is not treated in much detail in literature. Therefore, the effect of mutual addition of Cu and Fe on microstructural, thermo-mechanical, electrical and corrosion properties of modified Mn–Co spinel obtained by electrophoretic co-deposition of three different precursors is here explored and discussed. Cu and Fe doped Mn–Co spinels are usually processed "ex situ", i.e. before the deposition process [10,24]. The use of EPD technique to simultaneously co-deposit the Mn–Co spinel and the dopants (Cu, Fe) by adding controlled amounts of CuO and Fe_2O_3 particles to the suspension represents the novelty of this work. Indeed, this is the first investigation to report a one-step electrophoretic co-deposition of three different precursors to process modified spinel protective coatings. This study therefore set out to assess the simultaneous effect of Cu and Fe on the functional properties of a dual phase Mn–Co spinel structure.

3

1. Experimental

1.1 Sample preparation

Electrophoretic deposition was performed on 0.3-mm-thick Crofer 22 APU steel (Cr = 23 wt.%, Mn = 0.45 wt.%, La = 0.1 wt.%, Ti = 0.06 wt.%, Si and Al < 0.05 wt.%, Fe = Bal.; VDM Metals, Verdohl, Germany); 15 x 15 mm coupons were cut from a steel plate and a 3-mm hole was punched on one edge of each sample to allow hanging in the oxidation furnace. The steel coupons were sonicated in acetone/ethanol mixture for 10 min prior to deposition.

Commercially available $Mn_{1.5}Co_{1.5}O_4$ (Fuelcellmaterials, USA, d_{50}=634 nm), Fe_2O_3 (Fluka, d_{50}= 75 nm) and CuO (Alfa Aesar, d_{50}= 526 nm) powder precursors were used to prepare the four EPD suspensions reported in Table 1 which were labelled respectively 5Fe5Cu, 10Fe10Cu, 10Fe5Cu and 5Fe10Cu. Oxide powders were dispersed in a 60 vol.% ethanol/ 40 vo.% deionised water solution according to the relative concentration of spinel precursors reported in Table 1, to reach a solid load of 37.5 gL^{-1}. Each suspension was stabilised for 30 min, alternating sonication and mechanical stirring prior to be used for deposition. EPD was performed by a three-electrode setup to coat both surfaces of the coupons and using stainless steel counter electrodes; uniform deposition was achieved applying 50 V deposition voltage for 30 s at a sample-electrode distance of 15 mm. The Mn–Co spinel is widely reported to undergo cathodic deposition, as it develops a positive surface charge (zeta potential around + 13 mV); also CuO particles have a positive zeta potential (+ 6 mV) [22]. On the other hand, Fe_2O_3 develops a negative surface charge in the selected ethanol/water suspension: as already proposed in our previous study, Fe_2O_3 particles can associate with the Mn–Co spinel particles due to electrostatic interaction, leading to cathodic deposition as well [23]. In the case of the present study, a possible co-deposition mechanism is proposed and schematically reported in Figure 1.
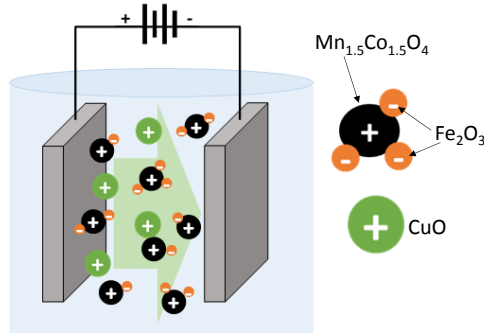
4

Figure 1: Schematic diagram showing the proposed co-deposition mechanism in the two-electrodes EPD set up.

After drying at room temperature, the coated coupons were sintered following a two-step approach consisting of a first reduction treatment at 1000 °C for 2 h in flowing Ar/H_2 (2 vol.%) followed by a re-oxidation treatment in static air at 900 °C for 2 h (heating and cooling ramps 10 °C/min).

To evaluate the effect of mutual addition of various amounts of Cu and Fe on the thermo-mechanical properties of the modified spinels by dilatometric analysis, cylindrical pellets of different compositions were prepared by mixing commercially available $Mn_{1.5}Co_{1.5}O_4$ (Fuelcellmaterials, USA, d_{50}=634 nm), Fe_2O_3 (Fluka, d_{50}= 75 nm) and CuO (Alfa Aesar, d_{50}= 526 nm) powders. The selected spinel precursors were weighted in stoichiometric amount to obtain the compositions labelled in Table 1 and mixed on rotating rollers for 24 hours; for each pellet, 2.5 g of powder precursors were prepared. As reported in Table 1, in addition to the aforementioned compositions used for the EPD suspensions (5Fe5CuMCO, 10Fe10CuMCO, 10Fe5CuMCO and 5Fe10CuMCO) pellets consisting of 100 wt.% pristine $Mn_{1.5}Co_{1.5}O_4$ spinel (MCO) were produced as benchmark; moreover, spinel pellets modified respectively with 5 wt.% and 10 wt.% of either Fe_2O_3 (5Fe and 10Fe) or CuO (5Cu and 10Cu) were produced to assess the influence of single element doping. After mixing, the precursors powders were placed in alumina boxed and subjected to the same sintering treatment as for EPD coatings (reduction in Ar/H_2 2 vol.%, 1000 °C, 2 h followed by re-oxidation in air, 900 °C, 2 h) during which the precursor

5

oxides react to form the modified spinels. Afterwards, obtained powders were pressed by uniaxial cold pressing in cylindrical pellets of 15 mm diameter and around 5 mm thickness, (suitable for dilatometric analysis). Pellets were sintered for 5 h at 1100 °C in air, followed by annealing at 800 °C for 2 h (heating and cooling rate 2 °C/min).

Table 1: Samples labelling, relative amount of spinel precursors and final compositions of the prepared spinels.

Sample label	Spinel precursors	Spinel composition
5Fe5Cu	90 wt.% $Mn_{1.5}Co_{1.5}O_4$ 5 wt.% Fe_2O_3 5 wt.% CuO	$Mn_{1.35}Co_{1.35}Fe_{0.15}Cu_{0.15}O_4$
10Fe10Cu	80 wt.% $Mn_{1.5}Co_{1.5}O_4$ 10 wt.% Fe_2O_3 10 wt.% CuO	$Mn_{1.20}Co_{1.20}Fe_{0.30}Cu_{0.30}O_4$
10Fe5Cu	85 wt.% $Mn_{1.5}Co_{1.5}O_4$ 10 wt.% Fe_2O_3 5 wt.% CuO	$Mn_{1.28}Co_{1.28}Fe_{0.29}Cu_{0.15}O_4$
5Fe10Cu	85 wt.% $Mn_{1.5}Co_{1.5}O_4$ 5 wt.% Fe_2O_3 10 wt.% CuO	$Mn_{1.28}Co_{1.28}Fe_{0.15}Cu_{0.29}O_4$
MCO	100wt.% $Mn_{1.5}Co_{1.5}O_4$	$Mn_{1.5}Co_{1.5}O_4$
5Fe	95 wt.% $Mn_{1.5}Co_{1.5}O_4$ 5 wt.% Fe_2O_3	$Mn_{1,43}Co_{1,43}Fe_{0,14}O_4$
10Fe	90 wt.% $Mn_{1.5}Co_{1.5}O_4$ 10 wt.% Fe_2O_3	$Mn_{1,35}Co_{1,35}Fe_{0,30}O_4$
5Cu	90 wt.% $Mn_{1.5}Co_{1.5}O_4$ 5 wt.% CuO	$Mn_{1,43}Co_{1,43}Cu_{0,14}O_4$
10Cu	90 wt.% $Mn_{1.5}Co_{1.5}O_4$ 10 wt.% CuO	$Mn_{1,35}Co_{1,35}Cu_{0,30}O_4$

1.2 Characterization

The oxidation kinetics of coated Crofer 22 APU was evaluated by thermogravimetric test in static air at 750 °C for 1000 h in total; every 250 h the furnaced was cooled down and the sample weighted (Radwag analytical balance with an accuracy of 1.0 x 10^{-6}) to evaluate the mass gain after every thermal cycle and compared to the as-sintered samples. For each coating composition, 4 coated coupons were treated in the oxidation furnace.

To characterize electrical properties of the coating at high temperature, area specific resistance (ASR) measurements were performed. Circle shaped platinum contacts with a diameter of 5 mm were applied on both sides of the spinel coated samples. The measurement was carried out in a four-electrode system. The sample was heated up to 750 °C, and then cooled to 200 °C with simultaneous impedance measurement every 50 °C. Area specific resistance was calculated according to the following equation:

$$ASR = \frac{R\ A}{2}$$

where: R-measured resistance [Ω], A- surface of the platinum contact [cm^2]. Electrical tests were performed using a tube furnace with stagnant air atmosphere and a potentiostat (Gamry Interface 1000 Potentiostat/Galvanostat/ZRA, Warminster, PA, USA).

The X-ray diffraction (XRD) patterns were obtained using a Bruker D8 diffractometer with Cu-Kα radiation; the patterns were recorded at room temperature in a 2θ range of 10°-70°, with a step size of 0.02626° and time per step of 10.20 s; recorded patterns were analysed using PanAlytical X'Pert software. The microstructures and compositions of the coated samples were examined using a field-emission scanning electron microscope (FESEM; SupraTM 40, Zeiss, Oberkochen, Germany) equipped with an energy dispersive X-ray analyser (EDS, Bruker, Germany). To examine the cross sections of coated Crofer 22 APU coupons, both as-sintered and oxidised samples were embedded

in epoxy resin and polished up to 4000 SiC paper. Furthermore, as-sintered 10Fe10Cu and 5Fe5Cu coated steel samples were analysed by means of transmission electron microscopy (TEM). FIB lamellae for transmission electron microscopy analysis were prepared using NEON Cross- Beam 40EsB of ZEISS. TEM investigations were performed on high resolution, Titan Cubed G2 60–300 (FEI) – a probe Cs corrected (S)TEM, equipped with ChemiSTEM EDS system based on a four windowless Silicon Drift Detectors (Super X). STEM imaging was performed in high angle annular dark-field (HAADF) mode. Analysis of crystal structure (phase composition) was performed using TEM-SAED method supported by JEMS software.

The Coefficient of thermal expansion (CTE) was evaluated by dilatometric measurements (DIL 402 PC/4, Netzsch) on 5-mm-thick sintered pellets, from room temperature to 900°C with a heating rate of 5 °C/min. Average CTEs were calculated from 200 °C to 750 °C as:

$$CTE = \frac{1}{L_0}\frac{\Delta L}{\Delta T}$$

where L_0 is the initial length, ΔL is the length variation in the selected temperature range defined by ΔT. The dilatometric curves and CTEs reported were obtained as the average between 4 measurements for each kind of sample.

2. Results and discussion

2.1 Characterization of the as-prepared coatings

To evaluate the effectiveness of the selected sintering treatments, XRD patterns were collected on EPD deposited and sintered coatings, after both reduction and re-oxidation steps. XRD results after the reducing treatment are reported in Figure 2. Manganese cobaltite reduced into metallic Co and MnO for all the studied cases, in accordance with

data reported in literature [18]. CuO particles reduced to metallic Cu after the reduction treatment; the same phase was found by Molin et al. [21] for coatings produced by electrophoretic co-deposition of MCO with 5 and 10 wt.% CuO. The intensity of Cu phase in patterns of Figure 2 is low due to the small amount of copper oxide in the EPD suspension; however, the peaks are more visible for samples with higher Cu addition (i.e. 10Fe10Cu and 5Fe10Cu). Interestingly, no phases associated with Fe were identified in the XRD patterns of Figure 2. In a previous work on Fe-doped coatings processed by electrophoretic co-deposition of MCO and Fe_2O_3, it was found that intermetallic phase $Co_{0.7}Fe_{0.3}$ formed for samples doped with 10 wt.% Fe_2O_3 [23] and that Fe addition lead to a shift of metallic Co peaks toward lower 2Theta angle. In this case, the intermetallic phase is not detected for Fe-Cu doped coatings, independently from the amount; however, closer inspection of the XRD pattern in the excerpt in Figure 2 b, shows that the shift of Co peaks is confirmed and it is more significant for coatings modified with the highest addition of Fe (i.e. 10Fe10Cu and 10Fe5Cu).
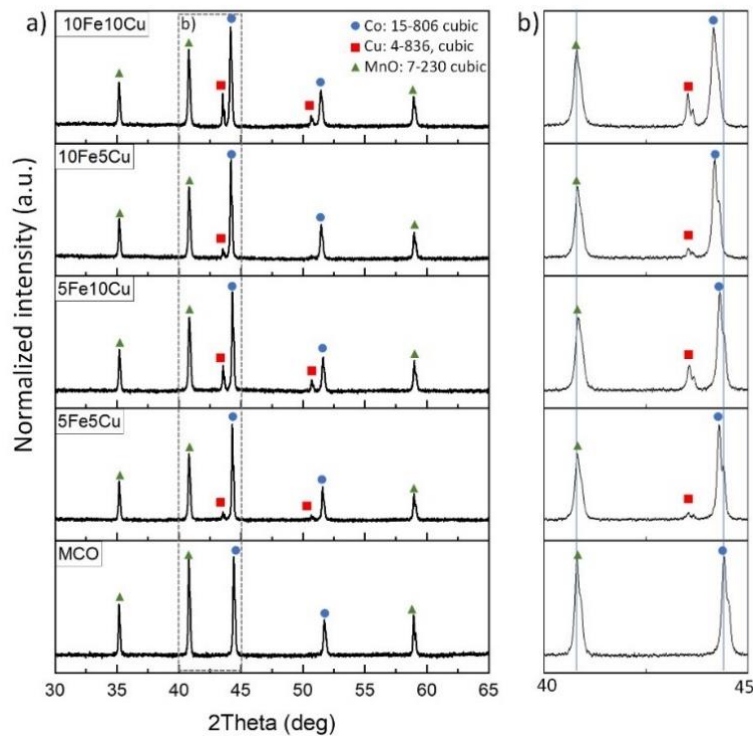

9

Figure 2: X-Ray diffraction patterns of the Fe and Cu doped coatings and pristine MCO after the reducing heat treatment. Patterns are normalized to the intensity of the highest peak. (b) Excerpt of patterns between 40° and 45°.

X-ray diffraction patterns after the re-oxidizing sintering step are presented in Figure 3 in comparison with the pattern recorded for pristine MCO spinel coating following the same sintering procedure. As expected, the pure MCO consist of a mixture of cubic and tetragonal spinel at room temperature; however, the main evidence is that all Fe-Cu doped coatings are composed of single-phase cubic spinel matching with the $MnCo_2O_4$ structure. This relevant result integrates and is consistent with data obtained in previous studies concerning in-situ doping of either Cu or Fe. Indeed, both Molin et al. [21] and Sabato et al. [22] reported a partial residual tetragonal spinel phase in coatings produced by EPD with the addition of CuO up to 10 wt.% in the suspension. Similarly, Zanchi et al. [23] showed that Fe-doped coatings determined lower intensity of the tetragonal phase with increasing the iron content, as well as a shift of the peaks of the cubic phase toward lower 2Theta angles: the evidence is explained by an increased cubic lattice parameter due to the substitution of Co by Fe, with larger ionic radii, in the octahedral sites. Similar hypotheses are confirmed by previous studies about Fe-doped spinels produced by ex-situ techniques [8,11,25]. As shown in Figure 3 b, Fe-Cu doped spinels exhibit the same shift of the cubic spinel already discussed; the shift results more significant for coatings containing higher percentage of iron (10Fe10Cu and 10Fe5Cu), confirming that Fe addition is the main responsible for the increase of the lattice parameter, even in the case of double Fe-Cu doping. Indeed, as proved by the study of Talic et al. [11], the single addition of Cu to the spinel does not lead to a consistent variation of the lattice parameter.

It is relevant to note that neither residual copper nor iron oxides are detected by XRD, meaning that the in-situ doping procedure is fully successful in producing modified spinel

layers. Therefore, the synergic effect of Fe and Cu completely stabilized the cubic structure of the spinel at room temperature.
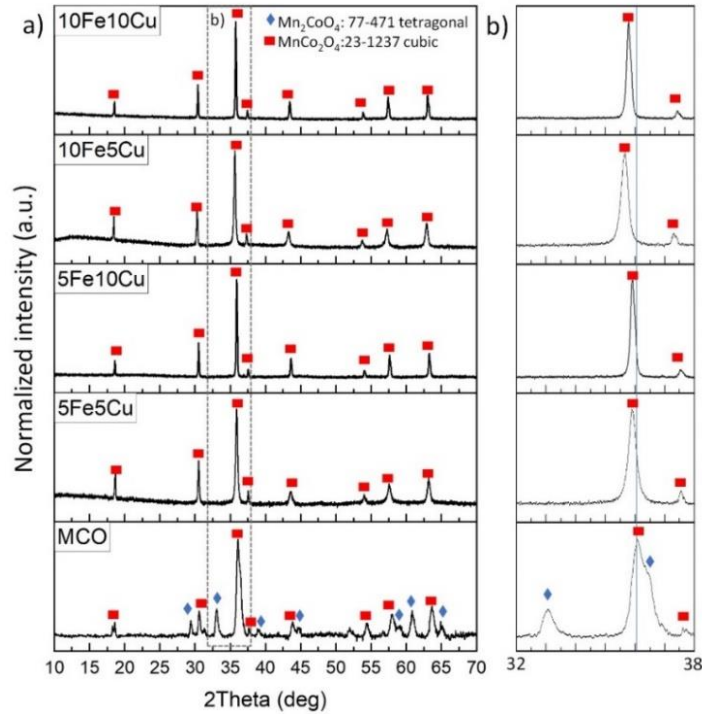
Figure 4 shows SEM cross-section images of produced coatings subjected to the two-step sintering. It is evident that all coatings adhere to the substrate very well and that there are no visible cracks or delamination phenomena at the coatings/steel interface. The thickness ranges between 10 and 15 μm, in agreement with the target of the electrophoretic co-deposition process. All the samples express very high densification, with the best result achieved by coatings with the highest Cu relative amount (i.e. 5Fe10Cu and 10Fe10Cu). Indeed, the beneficial effect on densification of Cu addition in the spinel is reported in previous studies [10,22]. Few pores of 3-5 μm dimension are present, but these are apparently closed porosity. EDS analysis confirmed that the three spinel precursors

($Mn_{1.5}Co_{1.5}O_4$, CuO and Fe_2O_3) in the EPD suspensions co-deposited homogeneously; indeed, EDS reported in Figure 4 and the calculated coating composition show only slightly variations from the nominal composition of the doped coatings (reported in Table 1). Moreover, the chosen sintering procedure did not lead to any Cr or Fe diffusion into the coatings during the heat treatments, as these elements were not present in the EDS results in any case.

a) 5Fe10Cu

EDS	O	Mn	Co	Fe	Cu
At.%	55.2	18.1	19.2	2.0	5.4

Comp. $Mn_{1.21}Co_{1.29}Fe_{0.13}Cu_{0.36}O_4$

b) 10Fe5Cu

EDS	O	Mn	Co	Fe	Cu
At.%	53.9	20.0	19.5	4.2	2.5

Comp. $Mn_{1.30}Co_{1.27}Fe_{0.27}Cu_{0.16}O_4$

c) 10Fe10Cu

EDS	O	Mn	Co	Fe	Cu
At.%	52.1	19.5	19.3	4.4	4.6

Comp. $Mn_{1.22}Co_{1.21}Fe_{0.28}Cu_{0.29}O_4$

d) 5Fe5Cu

EDS	O	Mn	Co	Fe	Cu
At.%	50.3	22.5	21.9	2.9	2.0

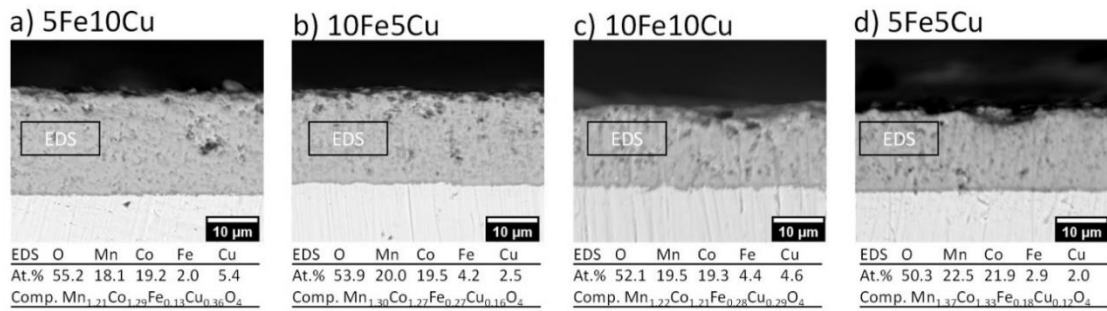Comp. $Mn_{1.37}Co_{1.33}Fe_{0.18}Cu_{0.12}O_4$

Figure 4: Cross section SEM (backscattered electron) images of the coatings after sintering, with semi-quantitative EDS results in at. % collected from the marked regions. The composition (Comp.) is calculated on the base of cations fractions, assuming the coatings are stoichiometric spinel oxides

In order to better understand the effect of simultaneous Fe and Cu doping on the spinel structure and morphology, a further examination of the microstructure was carried out using transmission electron microscopy (TEM) and selective area energy diffraction (SAED) on 10Fe10Cu and 5Fe5Cu as-sintered samples. Figure 5 shows results of TEM investigations on 10Fe10Cu as-sintered lamella. It is apparent that the coating is well adherent to the substrate. The elemental maps reported in Figure 5 a show that Mn, Co, Cu and Fe are homogeneously distributed in the coating. The intensity of Cu signal is partially overestimated due to interaction with the sample holder. The microstructure of the coating is better appreciable in Figure 5 b, where a BF image of the outer part of the coating is shown: the grains appear homogeneous in shape and dimension, thus confirming that the Fe-Cu modified is a single-phase spinel. As proved by SAED analysis

12

in point b1, the coating matches with the $MnCo_2O_4$ cubic spinel structure (zone axis 112).

On the other hand, in a previous work on in-situ Fe modified spinel, the coating was found

to be a mixture of elongated and larger grains, belonging respectively to the tetragonal

and cubic spinel structure [12]; similar evidences are highlighted in ref. [17] where a

$Mn_{1.5}Co_{1.5}O_4$ spinel coating was used. EDS analysis of the coating (Figure 5 b) shows

that the elemental concentration is fairly similar to the theoretic one. Indeed, the

calculated coating composition based of cation fractions and assuming the coatings are

stoichiometric spinel oxides is $Mn_{1.17}Co_{1.16}Fe_{0.27}Cu_{0.37}Cr_{0.02}O_4$ (nominal composition:

$Mn_{1.20}Co_{1.20}Fe_{0.30}Cu_{0.30}O_4$); the chromium concentration is negligible. As presented in

Figure 5 a and c, the interface with the substrate is characterised by the presence of a

densified coating layer, the reaction layer and the chromia scale. The reaction layer is the

result of the interdiffusion of Cr, Co and Mn, as confirmed by SAED in point 3c solved

by $CrMnCoO_4$ (zone axis 101). Interestingly, the first coating grain in contact with the

reaction layer (point c2 for SAED identification) matches with $MnCo_2O_4$ cubic spinel

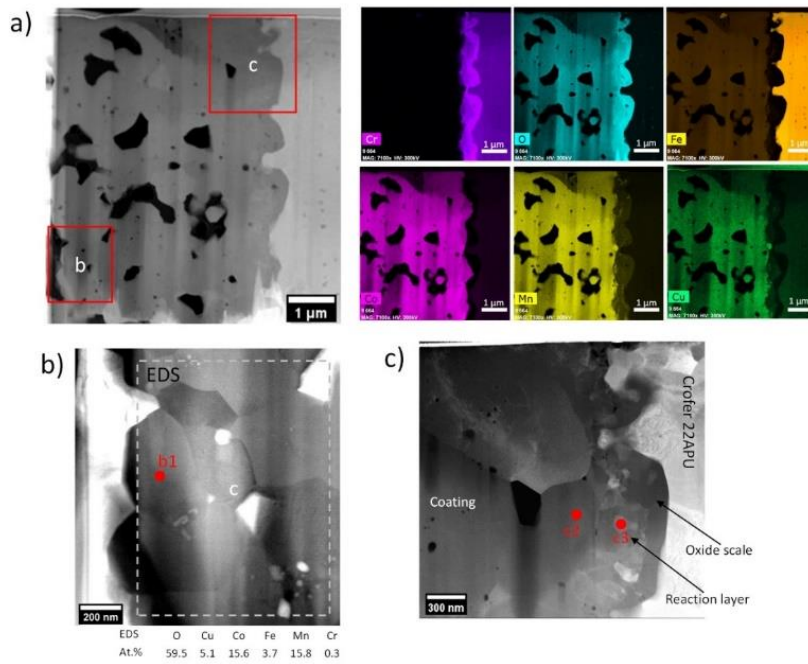structure (zone axis 112), as the outer part of the coating.

Figure 5: TEM images of 10Fe10Cu FIB lamella: a) HAADF image with EDS elemental analysis; b) BF TEM image from outer part of the coating with EDS quantification and marked point b1 for SAED analysis; c) BF TEM image from the coating-steel interface with marked point c2 and c3 for SAED analysis.

The morphology of the 5Fe5Cu outer part of the coating is reported in Figure 6, together with EDS elemental maps and quantification. The distribution of Mn, Co, Fe and Cu is completely homogeneous in this case as well, suggesting the formation of a single-phase spinel. Indeed, SAED in point a1 is solved by the cubic spinel structure $MnCo_2O_4$, as already disclosed by the XRD analysis. The calculated composition based on EDS cation distribution is $Mn_{1.28}Co_{1.27}Fe_{0.17}Cu_{0.23}Cr_{0.02}O_4$, very close to the nominal composition ($Mn_{1.35}Co_{1.35}Fe_{0.15}Cu_{0.15}O_4$).
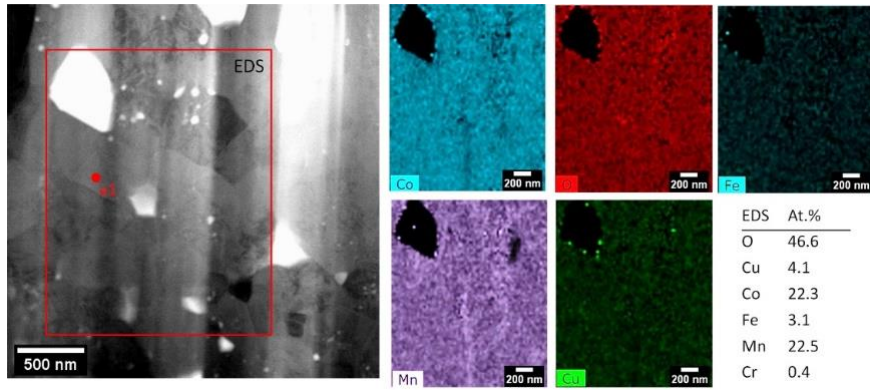
Figure 6: TEM images of 5Fe5Cu FIB lamella: BF TEM image with EDS elemental analysis and quantification from marked area and SAED from marked point a1.

2.2 Coefficient of thermal expansion

The evaluation of the coefficient of thermal expansion of the new modified spinels is crucial to assess their thermo-mechanical compatibility with the steel interconnect, to minimise the development of interfacial stress and avoid coating delamination during SOC stack operation. Figure 7 reports the coefficient of thermal expansion (CTE) calculated from 200 to 750 °C as a function of the iron content for all the analysed modified spinels. Furthermore, Figure 8 a-c shows dilatometric curves of all the studied spinels from room temperature to 900 °C; dilatometry curves are grouped as a function of Fe ratio as well. Each symbol and line in Figure 7 and Figure 8 represent the average obtained from 4 measurements of each kind of sample.

As displayed in Figure 7, at Fe 0 wt.% (corresponding to ordinate axis of the graph), the addition of Cu alone to the pristine spinel causes the progressive increase of the CTE, from 11.1 10^{-6} K^{-1} of MCO, 12.8 10^{-6} K^{-1} of 5Cu to 13.5 10^{-6} K^{-1} of 10Cu. Moreover, dilatometric curves in Figure 8 a show that MCO undergoes a phase transition between 500 and 550 °C, which corresponds to the transformation from tetragonal to cubic phase of the original $Mn_{1.5}Co_{1.5}O_4$ spinel. For 5Cu sample, the intensity of the same transition is significantly reduced, as confirmed by the fitting to the linear regression of the data (R^2

15

moves from 99.7% of MCO to 99.8% of 5Cu); with the addition of 10 wt.% Cu the transition is almost suppressed ($R^2 = 99.9\%$). These evidences support the results provided by Masi et al. [9] where the CTE at 800 °C of the dual-phase $Mn_{1.5}Co_{1.5}O_4$ is reported to increase from 9.7 10^{-6} K^{-1} to 13.5 10^{-6} K^{-1} of the cubic $MnCo_2O_4$. In this regard, the Cu addition is here proved to have the same effect in stabilizing the cubic phase of the spinel and in enhancing the overall CTE. The CTE increase due to Cu addition is explained by the preferential occupation of copper of tetrahedral sites in substitution of Co [26,27]: this substitution increases the number of elements in the lattice with different valence and therefore the CTE [8].

On the other hand, the single addition of Fe (samples labelled as 5Fe and 10Fe) to the $Mn_{1.5}Co_{1.5}O_4$ spinel overall decreases the CTE, but without following the same clear trend pointed out for Cu addition. In the case of iron doping, different data are reported in literature. Indeed, some studies suggest that iron preferably occupies octahedral sites instead of Co; due the greater ionic radius, Fe causes the increase of lattice parameter as well as the reduction of elements with different valence in the octahedral sites and lower CTE [8,25]. According to the observations of Talic et al. [11], iron replaces Co in the tetrahedral sites, due to the lower tendency of Fe to occupy octahedral sites than Co and Mn [28].

Another remarkable observation to emerge from these data is that when the ratio of iron is fixed to 5 wt.%, the CTE decreases up to 10.3 10^{-6} K^{-1}; however, when 5 wt.% or 10 wt.% Cu is included in the spinel composition (in 5Fe5Cu and 5Fe10Cu samples respectively) the CTE progressively increases until reaching slightly lower values compared to 5Cu and 10Cu samples (where no Fe is added). As shown in Figure 8 b, the dual-to-single phase transition is still partially visible for the 5Fe sample ($R^2 = 99.8\%$) between 500-550 °C, while it results almost completely suppressed for 5Fe5Cu and

5Fe10Cu samples (R^2= 99.9%). Similar trend is highlighted in Figure 8 c for 10Fe (R^2= 99.8%), 10Fe5Cu (R^2= 99.9%) and 10Fe10Cu (R^2= 99.9%) samples, but in this case the CTE difference between the samples is less significant, as the dilatometry curves are basically overlying. The same is appreciable in Figure 7 , where the CTE increases due to addition of both 5 wt.% and 10wt. % Cu to 10Fe sample which leads to a narrower range of CTE values. The fact that Fe-doping alone is not sufficient to fully suppress the double-phase transition is consistent with data obtained in [23].

The analysis of the dilatometry data reveals that Cu determines an increase of CTE, while Fe has the opposite effect: this property is better highlighted in Figure 8 d, when dilatometric curve of pristine MCO spinel is compared with 5 wt% iron doping (5Fe) and with 5 wt.% iron plus 10 wt.% copper doping (5Fe10Cu). Moreover, when both Cu and Fe are added to the spinel they express a synergic effect on the dilatometry behavior. As already suggested by Masi et al. [8], our study proves that the CTE of spinels can be tuned by tailoring the amount of different additional transition metals; the validity of the statement is here confirmed by evidence from a broader range of spinel compositions. Considering that the CTE reported for Crofer 22 APU at 700 °C is 11.6 10^{-6} K^{-1} and at 800 °C is 11.9 10^{-6} K^{-1} [29], the modified spinel that better matches the CTE of the steel substrate is the 10Fe5Cu composition.
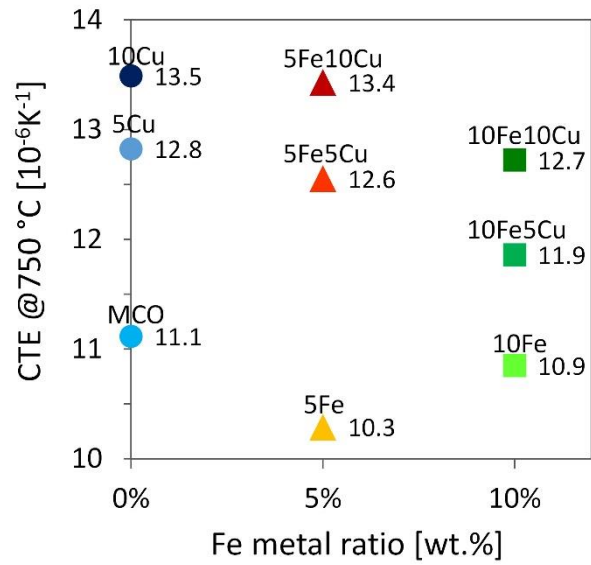
17

Figure 7: Coefficient of thermal expansion calculated at 750 °C as a function of Fe metal content.
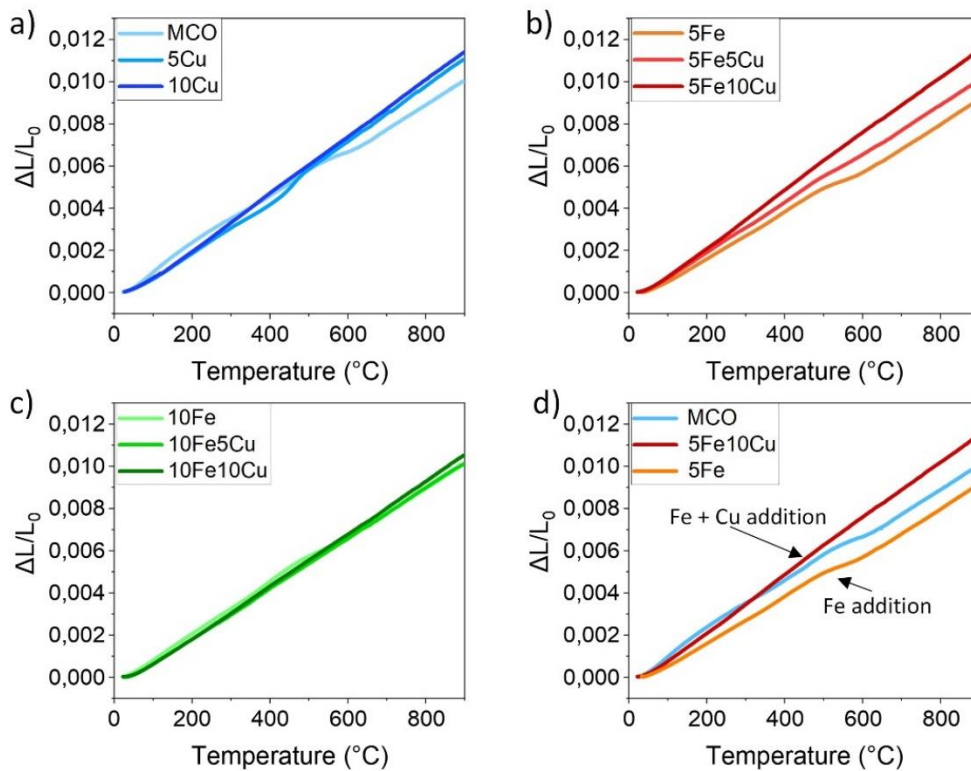

Figure 8: Dilatometric curves from room temperature to 900 °C of modified spinel pellets with a) 0 wt.% Fe, b) 5 wt.% Fe and c) 10 wt.% Fe; d) dilatometric curves of MCO, 5Fe and 5Fe10Cu samples.

2.3 Oxidation kinetics and electrical characterization of coatings

Oxidation performances of the different Fe-Cu doped spinels on Crofer 22 APU were evaluated up to 1000 h aging at 750 °C by thermogravimetric method. The mass gain during aging of each sample was measured cyclically. Considering that Crofer 22 APU coated by spinel coating has already been proved to follow parabolic oxidation [10,12,30], the mass gain results can be plotted in parabolic unit according to the following equation [31]:

$$\left(\frac{\Delta m}{A}\right)^2 = k_{p,m} \cdot t + C$$

where Δm is the measured mass gain [g] at a certain aging time (t) [s], A is the sample area [cm^2], C is an integration constant and $k_{p,m}$ is the parabolic rate constant [g^2 cm^{-4} s^{-1}]. Figure 9 reports the oxidation test results plotted in parabolic unit; $k_{p,m}$ corresponds to the slope of the trend lines. In order to neglect the contribution of the initial oxidation phenomena but considering only the steady state growth of the oxide scale, mass gain data from 0 to 250 h aging were not included in the calculation of the parabolic rate constant. The fitting to the linear regression line (R^2) is > 0.98 for 10Fe10Cu and 10Fe5Cu, but $R^2 < 0.98$ for 5Fe5Cu and 5Fe10Cu suggests that the oxidation could be not fully parabolic in this case.

Final mass gain data and calculated oxidation rate are reported in Table 2. Comparing the graph in Figure 9 and data in Table 2, it is apparent that the coating modified with 5% iron underwent the lowest oxidation, with the 5Fe10Cu samples reaching the best results. On the other hand, both samples with 10% Fe expressed higher oxidation phenomena: in particular, the coating with the highest quantity of modifying elements (i.e. 10Fe10Cu) showed the most significant mass gain and oxidation rate. As a comparison, oxidation results of bare Crofer 22 APU, unmodified MCO and 10Fe samples are reported in Table

2 as well: these data have already been published by Zanchi et al. [23] in a study ap to 2000 h aging at 750 °C; here data have been reported only to 1000 h aging. It is clearly appreciable that the Fe-Cu doped coatings of the present study remarkably reduce the oxidation phenomena not only compared to bare steel and MCO coating, but also to the 10Fe coating, that in [23] was identified as the best candidate. The reason of the evidence can be found in the synergic effect of both Fe and Cu in the spinel, leading to improved oxidation resistance and great coating densification.

Based on the mass gain till 1000 h aging, the theoretical oxide scale thickness can be calculated according to the following expression [10,31]:

$$\tau_{Cr_2O_3} = \frac{MW_{Cr_2O_3}}{48 \cdot \rho_{Cr_2O_3}} \cdot \left(\frac{\Delta m}{A}\right)$$

where τ is the Cr_2O_3 thickness, ρ is its density (5.21 g cm^{-3}), MW is its molar weight (152 g mol^{-1}), 48 is a factor for converting the oxygen mass in the Cr_2O_3 (i.e. 16×3) and $\frac{\Delta m}{A}$ is the mass gain at 1000 h. The obtained values are reported in Table 2; all the obtained oxide scale thickness are similar and very low, also compared to data reported in the previous study [23].
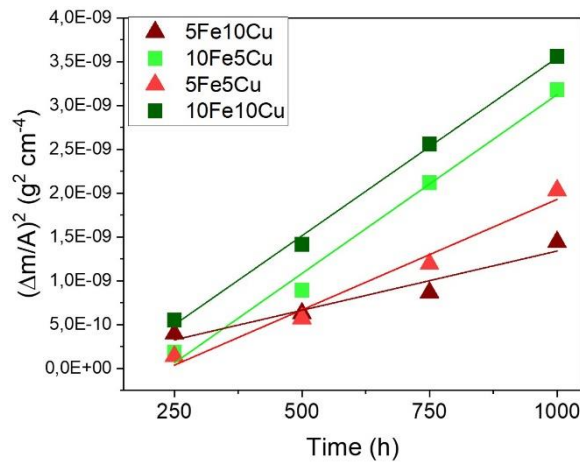

Figure 9: Parabolic rate plot with linear trend lines of coated Crofer 22 APU during cyclic oxidation at 750 °C in air (250–1000 h).

20

Table 2: Mass gain after 1000 h aging at 750 °C, oxidation rate Kp,m from 250 to 1000 h aging and calculated oxide scale thickness.

Sample	Mass gain 1000h [mg cm^{-2}]	$k_{p,m}$ [g^2 cm^{-4} s^{-1}]	Calculated oxide scale [μm]
10Fe10Cu	0.06 ± 0.005	1.0 × 10^{-15}	0.36
10Fe5Cu	0.06 ± 0.004	0.9 × 10^{-15}	0.36
5Fe5Cu	0.05 ± 0.008	0.6 × 10^{-15}	0.30
5Fe10Cu	0.04 ± 0.006	0.4 × 10^{-15}	0.24
Crofer 22 APU* [23]	0.24 ± 0.014	17.9 × 10^{-15}	1.46
MCO* [23]	0.18 ± 0.028	12.4 × 10^{-15}	1.09
10Fe* [23]	0.08± 0.004	2.7 × 10^{-15}	0.49

*Data of bare Crofer 22 APU, MCO and 10Fe are reported in Ref [23] **for 2000 h discontinuous aging at 750 °C in air; results have been here recalculated for 1000 h aging.**

Electrical characterization was conducted for all coated samples before aging (as-prepared samples) and after 1000 h discontinuous oxidation at 750 °C; results are summarised in Table 3 As expected, ASR after aging increased due to the development of the oxide scale, however, all the recorded values are very low: indeed all ASR are largely smaller that the threshold accepted for interconnect materials of 100 mΩ·cm^2 [32].

Figure 10 presents the temperature dependence of ASR (plotted in natural logarithm) during cooling between 750 and 550 °C; in this temperature range ASR follows a fairly linear trend, indicating the temperature-activated nature of electrical conduction for the studied systems and allowing to calculate the activation energy for electrical conductivity [33]:

$$\frac{ASR}{T} = Ae^{\left(\frac{E_A}{kT}\right)}$$

where A is a pre-exponential factor [Ω cm^2 K^{-1}], E$_A$ is the activation energy [eV], k is the Boltzmann's constant [eV K^{-1}] and T is the temperature [K].

The comparison of conductivity results with literature is not obvious, as measurements are strongly affected by the choice of test setup [18]; however, both ASR and the activation energies (Table 3) lay in the same range as reported by other studies and [10,12,24,32,34,35].

As shown in Figure 10 a, the ASR dependence over temperature does not express a clear trend depending on coatings composition for as-prepared samples. Samples aged for 1000 h at 750 °C (Figure 10 b) show that coatings with even amount of Fe and Cu (i.e. 5Fe5Cu and 10Fe10Cu) have lower electrical resistance at higher temperature. In particular, 5Fe5Cu composition confirmed the lowest ASR in both as-prepared and oxidised state. Moreover, the behaviour during cooling of respectively the two samples with 5 wt.% Fe (i.e. 5Fe5Cu and 5Fe10Cu) or 10 wt.% Fe (10Fe10Cu and 10Fe5Cu) results similar.
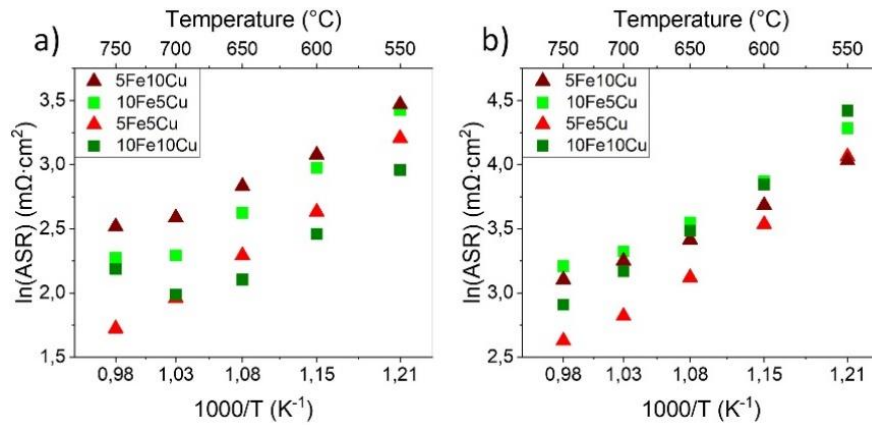

Figure 10: ASR dependence over temperature of a) as-prepared samples and b) 1000 h aged samples at 750°C

Table 3: ASR and activation energy determined for coatings deposited on Crofer 22 APU of as-prepared samples and after 1000 h cyclic oxidation in air at 750 °C

Sample	Before aging		After 1000 h aging @750°C		
	ASR @ 750 °C [mΩ x cm²]	Ea [eV]	ASR @ 750 °C [mΩ x cm²]	ASR increase [mΩ x cm²]	Ea [eV]
5Fe5Cu	5.6	0.57	13.8	+8.2	0.57
5Fe10Cu	12.4	0.40	22.3	+9.9	0.39
10Fe5Cu	9.7	0.49	24.8	+15.1	0.45
10Fe10Cu	8.9	0.36	18.3	+9.4	0.58

22

2.4 Post-mortem characterization

Figure 11 a-d shows SEM cross sections of different coatings after 1000 h discontinuous aging at 750°C. All coatings are fully continuous and well attached to the steel substrate confirming the good thermo-mechanical compatibility between Crofer 22 APU and the produced coatings, despite the thermal cycles during oxidation. All samples exhibit good densification, but coatings with higher copper relative amount reach the lowest residual porosity; in particular, 10Fe10Cu (Figure 11 c) results almost fully dense. On the other hand, the less densified coating is 10Fe5Cu, due to the greater Fe addition. The great densification of the coatings is certainly related to the choice of the two-step sintering treatment, as already found and discussed in previous studies [18,36]. Moreover, the enhanced sinterability due to copper addition is confirmed for Cu-doping alone as well [10,22]. On the other hand, Fe addition partially reduces the maximum densification reached in the coatings [12,23]. The oxide scale is visible as the darker-contrast layer at the interface between the steel substrate and coating, where few sub scale nodules are visible as well. The formation of these Mn-rich nodules is typical for high-temperature oxidation of Crofer 22 APU [12,17,23,37]. In agreement with the oxidation resistance test (showing very low mass increase related to oxygen uptake), the oxide scale is thin (< 0.5 μm)

Compositional analysis carried out by EDS presented in Figure 11 a-d shows the absence of Cr in the coatings, thus confirming the successful chromium retention capability for all produced compositions during oxidation. Moreover, EDS analysis r proves that coating compositions are preserved even after aging. Indeed, Figure 11 e reports X-ray diffraction patterns collected on the surface of samples after aging: as presented, all coatings exhibit the cubic spinel phase after 1000 h at 750°C and no formation of

secondary phases is detected, thus confirming the excellent stability of the processed Mn-Co-Cu-Fe coatings.
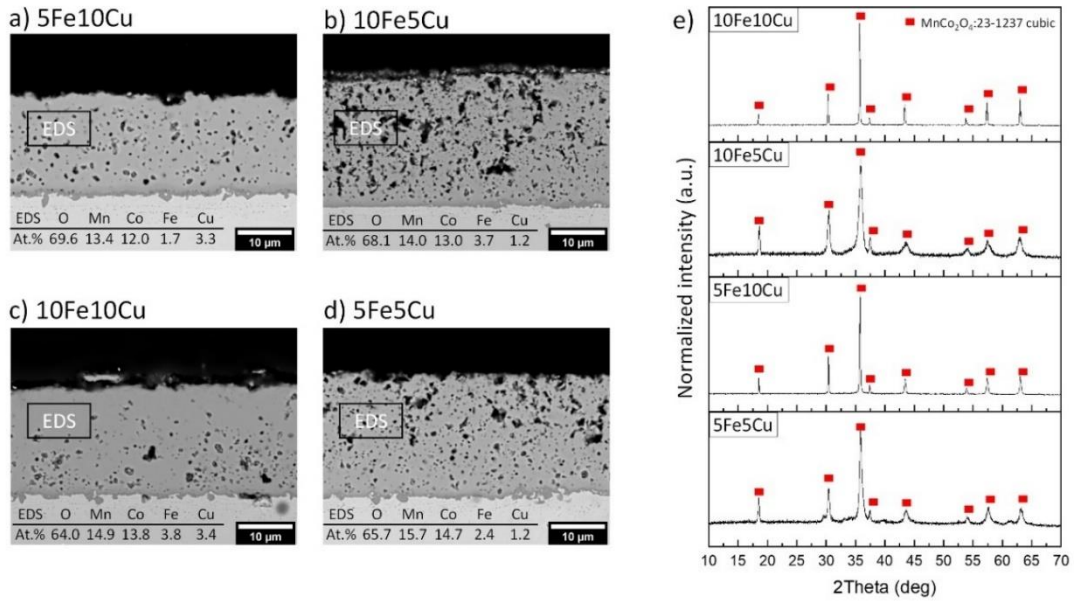

Figure 11: Cross section SEM (backscattered electron) images of the coatings after oxidation (1000 h, 750 °C, air) with semi-quantitative EDS results in at. % collected from the marked regions of coatings: a) 5Fe10Cu, b) 10Fe5Ccu, c)10Fe10Cu, d) 5Fe5Cu. e) XRD patters of studied coatings after oxidation.

3. Conclusions

The present study was designed to determine the effect of mutual addition of Cu and Fe on microstructural, thermo-mechanical, electrical and corrosion properties of modified Mn–Co spinels obtained by electrophoretic co-deposition of three different precursors. Evidences found in this work have confirmed EPD as a valuable method to design and produce in-situ modified spinel coatings through co-deposition of oxide precursors; the optimization of the two-step sintering treatment assured the formation of the spinel phase, stable even after 1000 h aging. This study has shown that Cu determines an increase of the overall CTE of the spinel, according to the percentage of copper addition; on the other hand, within the same sintering route, the addition of Fe has an opposite effect. The research has also demonstrated the synergic effect of the simultaneous Fe and Cu spinel

24

co-doping on tuning the thermo-mechanical properties of the spinel, an improved densification, as well as the stabilization of the $MnCo_2O_4$ cubic phase. All Fe-Cu doped coatings have demonstrated improved corrosion resistance at 750 °C, compared not only to uncoated and pristine Mn–Co spinel coated Crofer 22 APU, but also to Fe-doped coatings tested at the same conditions. Electrical properties have been confirmed to be satisfactory for the application of the coatings on stainless steel SOC interconnects. The findings reported here provide the first comprehensive assessment of simultaneous Cu and Fe addition into the Mn–Co spinel dual phase structure and lay the groundwork for future research into the tuning of Mn-based spinel properties. In the view of improving the durability, robustness and lowering the degradation and manufacturing costs of SOCs, a natural progression of this work is to explore the design of new spinel families, avoiding Co as critical raw material, by using EPD as a viable method to simultaneously deposit different precursors and to form the desired spinels by a reactive sintering.

References

[1]   S.M. Haile, Fuel cell materials and components, Acta Mater. 51 (2003) 5981–6000. https://doi.org/10.1016/j.actamat.2003.08.004.

[2]   Y.W. Chai, K. Kato, C. Yabu, S. Ishikawa, Y. Kimura, Disconnections and Laves (C14) precipitation in high-Cr ferritic stainless steels, Acta Mater. 198 (2020) 230–241. https://doi.org/10.1016/j.actamat.2020.08.006.

[3]   M. Palcut, L. Mikkelsen, K. Neufeld, M. Chen, R. Knibbe, P. V. Hendriksen, Corrosion stability of ferritic stainless steels for solid oxide electrolyser cell interconnects, Corros. Sci. 52 (2010) 3309–3320. https://doi.org/10.1016/j.corsci.2010.06.006.

[4]   J.A. Scott, D.C. Dunand, Processing and mechanical properties of porous Fe-26Cr-1Mo for solid oxide fuel cell interconnects, Acta Mater. 58 (2010) 6125–6133.

25

https://doi.org/10.1016/j.actamat.2010.07.030.

[5] M.A. Hassan, O. Bin Mamat, M. Mehdi, Review: Influence of alloy addition and spinel coatings on Cr-based metallic interconnects of solid oxide fuel cells, Int. J. Hydrogen Energy. (2020). https://doi.org/10.1016/j.ijhydene.2020.06.234.

[6] N. Shaigan, W. Qu, D.G. Ivey, W. Chen, A review of recent progress in coatings, surface modifications and alloy developments for solid oxide fuel cell ferritic stainless steel interconnects, J. Power Sources. 195 (2010) 1529–1542. https://doi.org/10.1016/j.jpowsour.2009.09.069.

[7] K.H. Tan, H.A. Rahman, H. Taib, Coating layer and influence of transition metal for ferritic stainless steel interconnector solid oxide fuel cell: A review, Int. J. Hydrogen Energy. 44 (2019) 30591–30605. https://doi.org/10.1016/j.ijhydene.2019.06.155.

[8] A. Masi, M. Bellusci, S.J. McPhail, F. Padella, P. Reale, J.-E. Hong, R. Steinberger-Wilckens, M. Carlini, The effect of chemical composition on high temperature behaviour of Fe and Cu doped Mn-Co spinels, Ceram. Int. 43 (2016) 2829–2835. https://doi.org/10.1016/j.ceramint.2016.11.135.

[9] A. Masi, M. Bellusci, S.J. McPhail, F. Padella, P. Reale, J.E. Hong, R. Steinberger-Wilckens, M. Carlini, Cu-Mn-Co oxides as protective materials in SOFC technology: The effect of chemical composition on mechanochemical synthesis, sintering behaviour, thermal expansion and electrical conductivity, J. Eur. Ceram. Soc. 37 (2017) 661–669. https://doi.org/10.1016/j.jeurceramsoc.2016.09.025.

[10] B. Talic, S. Molin, K. Wiik, P.V. Hendriksen, H.L. Lein, Comparison of iron and copper doped manganese cobalt spinel oxides as protective coatings for solid oxide fuel cell interconnects, J. Power Sources. 372 (2017) 145–156. https://doi.org/10.1016/j.jpowsour.2017.10.060.

26

[11]   B. Talic, P.V. Hendriksen, K. Wiik, H.L. Lein, Thermal expansion and electrical conductivity of Fe and Cu doped $MnCo_2O_4$spinel, Solid State Ionics. 326 (2018) 90–99. https://doi.org/10.1016/j.ssi.2018.09.018.

[12]   E. Zanchi, S. Molin, A.G. Sabato, B. Talic, G. Cempura, A.R. Boccaccini, F. Smeacetto, Iron doped manganese cobaltite spinel coatings produced by electrophoretic co-deposition on interconnects for solid oxide cells: Microstructural and electrical characterization, J. Power Sources. 455 (2020) 227910. https://doi.org/10.1016/j.jpowsour.2020.227910.

[13]   J.C.W. Mah, A. Muchtar, M.R. Somalu, M.J. Ghazali, Metallic interconnects for solid oxide fuel cell: A review on protective coating and deposition techniques, Int. J. Hydrogen Energy. 42 (2017) 9219–9229. https://doi.org/10.1016/j.ijhydene.2016.03.195.

[14]   S. Molin, A.G. Sabato, M. Bindi, P. Leone, G. Cempura, M. Salvo, S. Cabanas Polo, A.R. Boccaccini, F. Smeacetto, Microstructural and electrical characterization of Mn-Co spinel protective coatings for solid oxide cell interconnects, J. Eur. Ceram. Soc. 37 (2017) 4781–4791. https://doi.org/10.1016/j.jeurceramsoc.2017.07.011.

[15]   M. Sadl, O. Condurache, A. Bencan, M. Dragomir, U. Prah, B. Malic, M. Deluca, U. Eckstein, D. Hausmann, N.H. Khansur, K.G. Webber, H. Ursic, Energy-storage-efficient $0.9Pb(Mg_{1/3}Nb_{2/3})O_3–0.1PbTiO_3$ thick films integrated directly onto stainless steel, Acta Mater. 221 (2021) 117403. https://doi.org/10.1016/j.actamat.2021.117403.

[16]   B. Talic, A.C. Wulff, S. Molin, K.B. Andersen, P. Zielke, H.L. Frandsen, Investigation of electrophoretic deposition as a method for coating complex shaped steel parts in solid oxide cell stacks, Surf. Coatings Technol. 380 (2019) 1–8. https://doi.org/10.1016/j.surfcoat.2019.125093.

[17]   A.G. Sabato, E. Zanchi, S. Molin, G. Cempura, H. Javed, K. Herbrig, C. Walter, A.R. Boccaccini, F. Smeacetto, Mn-Co spinel coatings on Crofer 22 APU by electrophoretic deposition: Up scaling, performance in SOFC stack at 850 °C and compositional

27

modifications, J. Eur. Ceram. Soc. 41 (2021) 4496–4504. https://doi.org/10.1016/j.jeurceramsoc.2021.03.030.

[18] E. Zanchi, A.G. Sabato, S. Molin, G. Cempura, A.R. Boccaccini, F. Smeacetto, Recent advances on spinel-based protective coatings for solid oxide cell metallic interconnects produced by electrophoretic deposition, Mater. Lett. 286 (2021) 129229. https://doi.org/10.1016/j.matlet.2020.129229.

[19] E. Zanchi, J. Ignaczak, B. Kamecki, P. Jasiński, S. Molin, A.R. Boccaccini, F. Smeacetto, Manganese cobalt-based spinel coatings processed by electro- phoretic deposition method : the influence of sintering on deg- radation issues of Solid Oxide Cell oxygen electrodes at 750 ° C, Materials (Basel). 14 (2021) 3836. https://doi.org/10.3390/ma14143836.

[20] C.L. Martin, R.K. Bordia, The effect of a substrate on the sintering of constrained films, Acta Mater. 57 (2009) 549–558. https://doi.org/10.1016/j.actamat.2008.09.041.

[21] S. Molin, A.G. Sabato, H. Javed, G. Cempura, A.R. Boccaccini, F. Smeacetto, Co-deposition of CuO and Mn1.5Co1.5O4 powders on Crofer22APU by electrophoretic method: Structural, compositional modifications and corrosion properties, Mater. Lett. 218 (2018) 329–333. https://doi.org/10.1016/j.matlet.2018.02.037.

[22] A.G. Sabato, S. Molin, H. Javed, E. Zanchi, A.R. Boccaccini, F. Smeacetto, In-situ Cu-doped MnCo-spinel coatings for solid oxide cell interconnects processed by electrophoretic deposition, Ceram. Int. 45 (2019) 19148–19157. https://doi.org/10.1016/j.ceramint.2019.06.161.

[23] E. Zanchi, B. Talic, A.G. Sabato, S. Molin, A.R. Boccaccini, F. Smeacetto, Electrophoretic co-deposition of Fe2O3 and Mn1,5Co1,5O4: Processing and oxidation performance of Fe-doped Mn-Co coatings for solid oxide cell interconnects, J. Eur. Ceram. Soc. 39 (2019) 3768–3777. https://doi.org/10.1016/j.jeurceramsoc.2019.05.024.

28

[24] J. Ignaczak, Y. Naumovich, K. Górnicka, J. Jamroz, W. Wróbel, J. Karczewski, M. Chen, P. Jasiński, S. Molin, Preparation and characterisation of iron substituted Mn1.7Cu1.3-xFexO4 spinel oxides (x = 0, 0.1, 0.3, 0.5), J. Eur. Ceram. Soc. 40 (2020) 5920–5929. https://doi.org/10.1016/j.jeurceramsoc.2020.07.001.

[25] Y. Liu, J.W. Fergus, K. Wang, C. Dela Cruz, Crystal Structure, Chemical Stabilities and Electrical Conductivity of Fe-Doped Manganese Cobalt Spinel Oxides for SOFC Interconnect Coatings, J. Electrochem. Soc. 160 (2013) F1316–F1321. https://doi.org/10.1149/2.114311jes.

[26] P.A. Wright, S. Natarajan, J.M. Thomas, P.L. Gai-Boyes, Mixed-Metal Amorphous and Spinel Phase Oxidation Catalysts: Characterization by X-ray Diffraction, X-ray Absorption, Electron Microscopy, and Catalytic Studies of Systems Containing Copper, Cobalt, and Manganese, Chem. Mater. 4 (1992) 1053–1065. https://doi.org/10.1021/cm00023a024.

[27] J. Xiao, W. Zhang, C. Xiong, B. Chi, J. Pu, L. Jian, Oxidation behavior of Cu-doped MnCo2O4 spinel coating on ferritic stainless steels for solid oxide fuel cell interconnects, Int. J. Hydrogen Energy. 41 (2016) 9611–9618. https://doi.org/10.1016/j.ijhydene.2016.03.051.

[28] D.S. McClure, The distribution of transition metal cations in spinels, J. Phys. Chem. Solids. 3 (1957) 311–317. https://doi.org/10.1016/0022-3697(57)90034-3.

[29] VDM-Metals, VDM ® Crofer 22 APU, (2010). https://www.vdm-metals.com/fileadmin/user_upload/Downloads/Data_Sheets/Datenblatt_VDM_Crofer_22_APU.pdf (accessed April 2, 2019).

[30] B. Talic, H. Falk-Windisch, V. Venkatachalam, P.V. Hendriksen, K. Wiik, H.L. Lein, Effect of coating density on oxidation resistance and Cr vaporization from solid oxide fuel cell interconnects, J. Power Sources. 354 (2017) 57–67. https://doi.org/10.1016/j.jpowsour.2017.04.023.

[31]   D.J. Young, High Temperature Oxidation and Corrosion of Metals, volume 1, Elsevier, 2008. https://doi.org/10.1016/C2014-0-00259-6.

[32]   M. Bednarz, S. Molin, M. Bobruk, M. Stygar, E. Długoń, M. Sitarz, T. Brylewski, High-temperature oxidation of the Crofer 22 H ferritic steel with Mn1.45Co1.45Fe0.1O4 and Mn1.5Co1.5O4 spinel coatings under thermal cycling conditions and its properties, Mater.   Chem.   Phys.   225   (2019)   227–238. https://doi.org/10.1016/j.matchemphys.2018.12.090.

[33]   Z. Yang, K.S. Weil, D.M. Paxton, J.W. Stevenson, Selection and Evaluation of Heat-Resistant Alloys for SOFC Interconnect Applications, J. Electrochem. Soc. 150 (2003) A1188. https://doi.org/10.1149/1.1595659.

[34]   A. Kruk, M. Stygar, T. Brylewski, Mn–Co spinel protective–conductive coating on AL453 ferritic stainless steel for IT-SOFC interconnect applications, J. Solid State Electrochem. 17 (2013) 993–1003. https://doi.org/10.1007/s10008-012-1952-8.

[35]   T. Brylewski, S. Molin, M. Marczyński, Mazur, K. Domaradzki, O. Kryshtal, A. Gil, Influence of Gd deposition on the oxidation behavior and electrical properties of a layered system consisting of Crofer 22 APU and MnCo2O4 spinel, Int. J. Hydrogen Energy. 46 (2021) 6775–6791. https://doi.org/10.1016/j.ijhydene.2020.11.169.

[36]   M. Bobruk, S. Molin, M. Chen, T. Brylewski, P.V. Hendriksen, Sintering of MnCo2O4 coatings prepared by electrophoretic deposition, Mater. Lett. 213 (2018) 394–398. https://doi.org/10.1016/j.matlet.2017.12.046.

[37]   M. Stanislowski, E. Wessel, K. Hilpert, T. Markus, L. Singheiser, Chromium Vaporization from   High-Temperature   Alloys,   J.   Electrochem.   Soc.   154   (2007)   A295. https://doi.org/10.1149/1.2434690.

Declaration of interests

☒ The authors declare that they have no known competing financial interests or personal relationships that could have appeared to influence the work reported in this paper.

☐The authors declare the following financial interests/personal relationships which may be considered as potential competing interests: